Electron Spin Polarization Transfer to the Charge-Separated State from Locally Excited Triplet Configuration. Theory and Its Application to Characterization of Geometry and Electro...

ARTICLE *in* THE JOURNAL OF PHYSICAL CHEMISTRY B · NOVEMBER 2010

Impact Factor: 3.3 · DOI: 10.1021/jp102330a · Source: PubMed

3 AUTHORS, INCLUDING:

Yasuhiro Kobori
Kobe University
48 PUBLICATIONS **836** CITATIONS
SEE PROFILE

Hisao Murai
Shizuoka University
109 PUBLICATIONS **1,376** CITATIONS
SEE PROFILE

Electron Spin Polarization Transfer to the Charge-Separated State from Locally Excited Triplet Configuration: Theory and Its Application to Characterization of Geometry and Electronic Coupling in the Electron Donor−Acceptor System†

Yasuhiro Kobori,* Masaaki Fuki, and Hisao Murai

Department of Chemistry, Faculty of Science, Shizuoka University, 836 Ohya Surugaku, Shizuoka 422-8529 Japan

Received: March 15, 2010; Revised Manuscript Received: May 11, 2010

We present a theoretical model of analysis of the time-resolved electron paramagnetic resonance (TREPR) spectrum of the charge-separated (CS) state generated by the photoinduced electron transfer (ET) reaction via the locally excited triplet state in an electron donor−acceptor (D−A) system with a fixed molecular orientation. We show, by the stochastic−Liouville equation, that chemically induced dynamic electron polarization (CIDEP) of the triplet mechanism is explained by lack of transfer of quantum coherence terms in the primary triplet spin state, resulting in net emissive or absorptive electron spin polarization (ESP) which is dependent on anisotropy of the singlet−triplet intersystem crossing in the precursor excited state. This disappearance of the coherence is clearly shown to occur when the photoinduced ET rate is smaller than the angular frequency of the Zeeman splitting: the transferred coherence terms are averaged to be zero due to effective quantum oscillations during the time that the chemical reaction proceeds. The above theory has been applied to elucidate the molecular geometries and spin−spin exchange interactions ($2J$) of the CS states for both folded and extended conformers by computer simulations of TREPR spectra of the zinc porphyrin−fullerene dyad (ZnP−C_{60}) bridged by diphenyldisilane. On the extended conformation, the electronic coupling is estimated from the $2J$ value. It has been revealed that the coupling term is smaller than the reported electronic interactions of the porphyrin−C_{60} systems bridged by diphenylamide spacers. The difference in the electronic couplings has been explained by the difference in the LUMO levels of the bridge moieties that mediate the superexchange coupling for the long-range ET reaction.

Introduction

For development of the molecular solar energy conversion systems, it is crucial to investigate how both the molecular geometry and the electronic structure of electron donor−acceptor (D−A) molecules contribute to the electronic coupling for the charge-separation (CS) and for the charge-recombination (CR) processes.[1–7] A wide variety of D−A molecules have been synthesized and extensively investigated to mimic the efficient light−energy conversion systems of the natural photosynthetic reaction centers (PRCs).[1,2,8–12] The PRCs undergo the efficient stepwise CS processes[13] initiating from the photoexcited singlet configurations of a pigment.

The time-resolved EPR (TREPR) method has been a powerful tool to investigate several photochemical processes. By using the TREPR, electron spin polarization (ESP) has been observed at nanosecond and microsecond regions on radicals, radical pairs, excited triplet states, and so on.[4,14–34] Basically, the ESP is a signature of the primary photochemical processes,[35] and several ESP mechanisms have been established to account for non-Boltzmann spin distributions of the reaction intermediates observed by the TREPR technique.[36] The ESP mechanisms have been utilized to characterize the photochemical processes and the electronic properties in the photosynthetic proteins,[24,37–46] the electronic molecular wires,[30–32] and so on. Molecular geometries of the CS states have been examined in detail using the TREPR method by analyzing the ESP of the spin-correlated radical pair (SCRP) for several PRCs[24,37–46] and for the artificial D−A systems[3,7] in which the singlet precursor CS reactions are predominant. Contrarily, only a few studies have been performed to elucidate the molecular conformations and the exchange interactions in the CS states of the D−A systems in which the photoinduced CS reactions take place via the excited triplet configurations.[4,28,33]

The photoexcited triplet states are well-known to possess characteristic anisotropic properties in the spin system. Rates of the singlet−triplet intersystem crossing (ISC) to the three spin sublevels of X, Y, and Z in the excited triplet state are anisotropic according to the spin−orbit coupling interaction.[47] The spin−spin dipolar interaction (or zero-field splitting interaction) in the triplet state is strongly dependent on the direction of the magnetic field (B_0) with respect to the principal axes (X, Y, and Z) of the triplet spin configuration.[47] Transfer of the ESP in the precursor triplet state takes place to the spin states of the radical pair during the CS reaction when the spin−lattice relaxation of the polarized triplet state is slower than the reaction.[4,26] Thus, in principle, the anisotropic triplet characters should be quite powerful to determine the molecular geometry and the electronic properties in the CS state of $D^{+\bullet}A^{-\bullet}$ in detail by using the TREPR method.[4]

Electron spin polarization transfer (ESPT) phenomena have been investigated in several photochemical systems by the TREPR.[4,21,22,26,34,48–50] To account for the TREPR spectra obtained by the triplet−triplet (TT) energy transfer and by the triplet−precursor photoinduced ET processes, the ESPT mechanisms have been discussed in terms of the conservation of the spin angular momentum: since the operators responsible for the electronic couplings of the reactions have no effect on the

† Part of the "Michael R. Wasielewski Festschrift".

* Corresponding author. E-mail: sykobor@ipc.shizuoka.ac.jp.

10.1021/jp102330a
Published on Web 05/28/2010

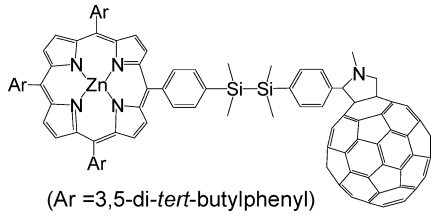

Figure 1. Structural formula of ZnP−C_{60} bridged by diphenyldisilane.

electron spin, the transferred populations in the triplet spin sublevels have been supposed to be equal to the probabilities, finding the characters of the basis spin wave functions of the precursor triplet sublevels.[4,21,22,26,48,50] However, adequate theoretical treatments are required in the ESP calculations not only on the sublevel populations but also on the coherence terms in the spin systems in the precursor states.[3,24,44–46,51] To our knowledge, no studies have investigated how the coherence terms in the excited triplet states contribute to the observed triplet spin polarization during the triplet−triplet ESPT processes.

In this paper, we show by the stochastic−Liouville equation (SLE) that, through the photoinduced ET processes via the excited triplet configuration, the quantum coherences generated in the primary triplet state in the presence of the magnetic field can be transferred to the population terms in the triplet radical pair state (or SCRP) that is detected by the TREPR. Also, the triplet mechanism CIDEP[34] effect, by which the net emissive or absorptive polarization is generated in the CS state, is explained by lack of transfer of the quantum coherence terms in the primary triplet spin states. By using the density matrix formalism, it is shown that the condition in which the quantum coherence is transferred is simply determined by the rate constant of the chemical processes. By the computer simulations of the TREPR spectra of the photoinduced CS state of the linked system of the zinc porphyrin−fullerene dyad (ZnP−C_{60}) bridged by diphenyldisilane (Figure 1),[4] the above theory is tested. Molecular geometries and the spin−spin exchange interactions of the CS states for both folded and extended conformers are determined.

Experimental Section

Samples. Benzonitrile (>98%, Wako) was used as received. The fullerene−porphyrin dyad (ZnP−C_{60}) linked with the diphenyldisilane bridge was synthesized as reported previously.[52] For the TREPR measurement, the concentration of ZnP−C_{60} was 2×10^{-4} M.

Time-Resolved EPR. The X-band TREPR measurements were carried out using a Bruker EMX system. In the microwave bridge, a modified preamplifier (ER047PH) in which the time resolution is enhanced (~60 ns) was equipped. Light excitations were performed by the second harmonic (532 nm) of a Nd: YAG laser (Continuum, Minilite II, fwhm ~5 ns). Transient signals were averaged by a digital oscilloscope (Tektronix, TDS 520D) at 201 different external magnetic field positions and were transferred to a personal computer via a GPIB communication to obtain the 2-dimentional TREPR data. Temperature was controlled by a nitrogen-gas flow system. The nitrogen gas was flowed through a liquid-nitrogen container and was transferred to a sample dewar inserted in a microwave cavity. Temperature was controlled by the flow rate of the nitrogen gas.

Theory and Computation Method

A. Triplet−Triplet ESPT Model. Figure 2 shows schematic representation of the ESPT through the photoinduced ET from

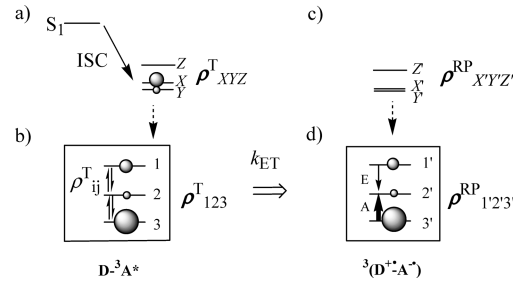

Figure 2. Schematic representations of ESPT by the intramolecular photoinduced ET in the D−A linked system. (a) Anisotropy of the intersystem crossing (ISC) to generate the excited triplet state of D−^{3}A*. *X*, *Y*, and *Z* denote the triplet spin eigenfunctions at the zero field. (b) The triplet spin eigenstates of 1, 2, and 3 are shown in the presence of the external magnetic field for the excited triplet state as the reaction precursor. The population terms (ρ_{11}, ρ_{22}, and ρ_{33}) of the density matrix $\boldsymbol{\rho}^{T}_{123}$ are shown by balls on the sublevels, while the coherence terms (ρ^{T}_{ij}) are represented by arrows between the sublevels. (c) The triplet spin eigenfunctions (*X*′, *Y*′, and *Z*′) of the CS state of ^{3}(D$^{+\bullet}$−A$^{-\bullet}$) at the zero field. (d) Triplet spin sublevels of 1′, 2′, and 3′ in ^{3}(D$^{+\bullet}$−A$^{-\bullet}$) are shown in the presence of the magnetic field and are represented by the linear combinations of the eigenfunctions of *X*′, *Y*′, and *Z*′. The ESP or the population ($\rho_{1'1'}$, $\rho_{2'2'}$, and $\rho_{3'3'}$) in $\boldsymbol{\rho}^{RP}_{1'2'3'}$ varies with the rate constant (k_{ET}) of the CS reaction. When $k_{TT} < g\beta B_0/\hbar$, the coherence terms are averaged to zero, resulting in the net absorptive (or emissive) triplet mechanism ESP represented by $\rho_{1'1'} - \rho_{3'3'} \approx \rho_{11} - \rho_{33}$ from eq 34.

the excited triplet state of D−^{3}A* to the CS state of D$^{+\bullet}$−A$^{-\bullet}$. After the light excitation of the linked D−A molecule, the S_1−T_1 ISC by the spin−orbit coupling produces the excited triplet state D−^{3}A* with different population rates to the triplet sublevels[47] (Figure 2a) of $|X\rangle = |\beta\beta - \alpha\alpha\rangle/\sqrt{2}$, $|Y\rangle = i|\beta\beta + \alpha\alpha\rangle/\sqrt{2}$, and $|Z\rangle = |\alpha\beta + \beta\alpha\rangle/\sqrt{2}$ that diagonalize the spin dipolar interaction in the excited triplet state with the eigenvalues of *X*, *Y*, and *Z*. Figure 2b shows the triplet spin eigenstates (1, 2, and 3) represented on the basis functions in the presence of the magnetic field. Since the eigenstates (1, 2, and 3) are expressed as the linear combinations of the eigenfunctions of *X*, *Y*, and *Z*, the populations and the coherences in levels in 1, 2, and 3 are affected by the initial populations in the *XYZ* system. The triplet wave functions in the CS state can also be represented as shown in Figure 2c and Figure 2d in the absence and in the presence of the magnetic field, respectively. The singlet spin can participate in the CS state when the spin−spin exchange coupling is weak. This participation of the singlet character is considered in the following section as the spin-correlated radical pair. In this section, only the triplet character in the CS state is considered using the 3×3 density matrix on the basis of the triplet sublevels to clearly understand the triplet−triplet ESPT phenomena. (Figure 2). One should note that the principal axes of *X*′, *Y*′, and *Z*′ in the CS state are generally different from the principal axes *X*, *Y*, and *Z*. Figure 3 shows an example of the molecular geometry of a dyad of the zinc porphyrin-bridge−C_{60} (ZnP−C_{60}) system investigated in this study. In the precursor excited triplet state of ZnP−$^3C_{60}$*, the principal axes (*X*, *Y*, and *Z*) of the C_{60} moiety are shown by the black axes in Figure 3. In the triplet CS state, the *Z*′ principal axis is parallel to the direction between the two radical species as shown by a green axis in Figure 3. In this study, the point-dipole approximation is considered for the spin dipolar interaction of the CS state. The zero-field basis functions are related as follows

$$\begin{pmatrix} |X'\rangle \\ |Y'\rangle \\ |Z'\rangle \end{pmatrix} = \mathbf{U}_{M'}^{-1} \begin{pmatrix} |X\rangle \\ |Y\rangle \\ |Z\rangle \end{pmatrix} \quad (1)$$

where

$$\mathbf{U}_{M'} = \begin{pmatrix} a_{X'X} & a_{Y'X} & a_{Z'X} \\ a_{X'Y} & a_{Y'Y} & a_{Z'Y} \\ a_{X'Z} & a_{Y'Z} & a_{Z'Z} \end{pmatrix} \quad (2)$$

where each element a_{KL} represents direction cosine between the principal axes. As shown in Figure 3, the direction of the Z' axis is set by θ and ϕ using the polar angles with respect to the Z and the X axis, respectively. Under the point-dipole approximation, since the X' axis is equivalent to the Y' axis, the X' axis can be set to be lying in the $X-Y$ plane. In this case, $\mathbf{U}_{M'}$ is represented as follows

$$\mathbf{U}_{M'} = \begin{pmatrix} \sin\phi & \cos\theta\cos\phi & \sin\theta\cos\phi \\ -\cos\phi & \cos\theta\sin\phi & \sin\theta\sin\phi \\ 0 & -\sin\theta & \cos\theta \end{pmatrix} \quad (3)$$

To compute the populations in the CS state (Figure 2d), we need to obtain the density matrix for the CS state on the basis of the 1′, 2′, and 3′ levels that diagonalize the spin Hamiltonian in the CS state. Also, we need to determine a transformation matrix $\mathbf{U}_{CS}$ between the 123 system and the 1′2′3′ system shown below

$$\begin{pmatrix} |1'\rangle \\ |2'\rangle \\ |3'\rangle \end{pmatrix} = \mathbf{U}_{CS}^{-1} \begin{pmatrix} |1\rangle \\ |2\rangle \\ |3\rangle \end{pmatrix} \quad (4)$$

The spin Hamiltonian in the triplet CS state is represented as follows

$$\hat{\mathrm{H}}_{1'2'3'}^{RP} = \mathbf{U}_{RP}^{-1} \hat{\mathrm{H}}_{X'Y'Z'}^{RP} \mathbf{U}_{RP} = \begin{pmatrix} \omega_{1'} & & \\ & \omega_{2'} & \\ & & \omega_{3'} \end{pmatrix} \quad (5)$$

where $\mathbf{U}_{RP}$ denotes the unitary matrix composed of eigenvectors as

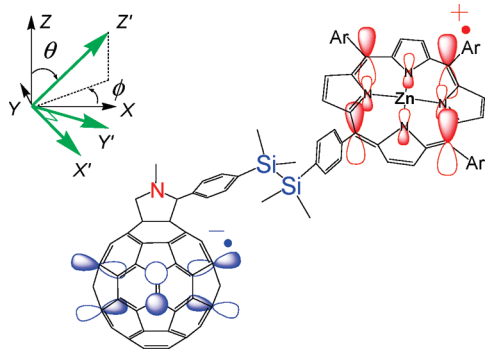

Figure 3. Molecular geometry of the extended conformation of the ZnP−C_{60} dyad linked by diphenyldisilane.

$$\mathbf{U}_{RP} = \begin{pmatrix} c_{1'X'} & c_{2'X'} & c_{3'X'} \\ c_{1'Y'} & c_{2'Y'} & c_{3'Y'} \\ c_{1'Z'} & c_{2'Z'} & c_{3'Z'} \end{pmatrix} \quad (6)$$

The eigenfunctions are represented as $|i'\rangle = c_{i'X}|X'\rangle + c_{i'Y}|Y'\rangle + c_{i'Z}|Z'\rangle$ (for $i' = 1'$, $2'$, and $3'$) of the CS state, that is

$$\begin{pmatrix} |1'\rangle \\ |2'\rangle \\ |3'\rangle \end{pmatrix} = \mathbf{U}_{RP}^{-1} \begin{pmatrix} |X'\rangle \\ |Y'\rangle \\ |Z'\rangle \end{pmatrix} \quad (7)$$

In eq 5, $\hat{H}_{X'Y'Z'}^{RP}$ is represented as[53]

$$\hat{\mathrm{H}}_{X'Y'Z'}^{RP} = \begin{pmatrix} X' & -ig\beta B_0\cos\theta_B & ig\beta B_0\sin\phi_B\sin\theta_B \\ ig\beta B_0\cos\theta_B & Y' & -ig\beta B_0\cos\phi_B\sin\theta_B \\ -ig\beta B_0\sin\phi_B\sin\theta_B & ig\beta B_0\cos\phi_B\sin\theta_B & Z' \end{pmatrix} \quad (8)$$

where $X' = D'/3$, $Y' = D'/3$, and $Z' = -(2/3)D'$. The E value is treated to be zero under the point-dipole approximation for the CS state. θ_B and ϕ_B are the polar angles of the external magnetic field B_0 with respect to the Z' and X' principal axes, respectively, in the zero-field splitting interaction. Similarly, the spin Hamiltonian in the excited triplet state is represented on the basis of 1, 2, and 3 systems as follows

$$\hat{\mathrm{H}}_{123}^{T} = \mathbf{U}_{T}^{-1} \hat{\mathrm{H}}_{XYZ}^{T} \mathbf{U}_{T} = \begin{pmatrix} \omega_1 & & \\ & \omega_2 & \\ & & \omega_3 \end{pmatrix} \quad (9)$$

where $\mathbf{U}_T$ denotes the unitary matrix composed of the eigenvectors as

$$\mathbf{U}_{T} = \begin{pmatrix} c_{1X} & c_{2X} & c_{3X} \\ c_{1Y} & c_{2Y} & c_{3Y} \\ c_{1Z} & c_{2Z} & c_{3Z} \end{pmatrix} \quad (10)$$

The eigenfunctions are represented as $|i\rangle = c_{iX}|X\rangle + c_{iY}|Y\rangle + c_{iZ}|Z\rangle$ (for $i = 1$, 2 and 3). $\hat{H}_{XYZ}^{T}$ is the spin Hamiltonian of the excited triplet state represented using the basis functions of $|X\rangle$, $|Y\rangle$, and $|Z\rangle$. (See eq 12.) ω_i represents eigenvalues for the energy levels of 1, 2, and 3. From eq 10, the following relation is obtained

$$\begin{pmatrix} |1\rangle \\ |2\rangle \\ |3\rangle \end{pmatrix} = \mathbf{U}_{T}^{-1} \begin{pmatrix} |X\rangle \\ |Y\rangle \\ |Z\rangle \end{pmatrix} \quad (11)$$

In eq 9, $\hat{H}_{XYZ}^{T}$ is obtained as

$$\hat{\mathrm{H}}_{XYZ}^{T} = \begin{pmatrix} X & 0 & 0 \\ 0 & Y & 0 \\ 0 & 0 & Z \end{pmatrix} + \mathbf{U}_{M'} \begin{pmatrix} 0 & -ig\beta B_0\cos\theta_B & ig\beta B_0\sin\phi_B\sin\theta_B \\ ig\beta B_0\cos\theta_B & 0 & -ig\beta B_0\cos\phi_B\sin\theta_B \\ -ig\beta B_0\sin\phi_B\sin\theta_B & ig\beta B_0\cos\phi_B\sin\theta_B & 0 \end{pmatrix} \mathbf{U}_{M'}^{-1} \quad (12)$$

where $X = D_T/3 - E_T$, $Y = D_T/3 + E_T$, and $Z = -(2/3)D_T$. From eqs 1, 7, and 11, $\mathbf{U}_{CS}$ in eq 4 is represented as

$$\mathbf{U}_{CS} = \mathbf{U}_T^{-1}\mathbf{U}_{M'}\mathbf{U}_{RP} \tag{13}$$

The density matrix ($\boldsymbol{\rho}^T$) for the spin state of D$-^3$A* and the density matrix ($\boldsymbol{\rho}^{RP}$) of the triplet CS state ^{3}(D$^{+\bullet}-$A$^{-\bullet}$) obey the stochastic−Liouville equation, as follows

$$\dot{\boldsymbol{\rho}}_{XYZ}^T = -i[\hat{\mathrm{H}}_{XYZ}^T, \boldsymbol{\rho}_{XYZ}^T] - k_{ET}\boldsymbol{\rho}_{XYZ}^T \tag{14}$$

$$\dot{\boldsymbol{\rho}}_{XYZ}^{RP} = -i[\hat{\mathrm{H}}_{XYZ}^{RP}, \boldsymbol{\rho}_{XYZ}^{RP}] + k_{ET}\boldsymbol{\rho}_{XYZ}^T \tag{15}$$

where subscript *XYZ* denotes the basis spin wave functions of *X*, *Y*, and *Z* as shown in Figure 2a, denoting that the matrix elements of the operators like $\boldsymbol{\rho}$ are represented on the basis of the spin functions of *X*, *Y*, and *Z*. By the Laplace transform of eqs 14 and 15, the following relation can be obtained

$$s\tilde{\boldsymbol{\rho}}_{XYZ}^T - \boldsymbol{\rho}_{XYZ}^T(0) = -i[\hat{\mathrm{H}}_{XYZ}^T, \tilde{\boldsymbol{\rho}}_{XYZ}^T] - k_{ET}\tilde{\boldsymbol{\rho}}_{XYZ}^T \tag{16}$$

$$s\tilde{\boldsymbol{\rho}}_{XYZ}^{RP} = -i[\hat{\mathrm{H}}_{XYZ}^{RP}, \tilde{\boldsymbol{\rho}}_{XYZ}^{RP}] + k_{ET}\tilde{\boldsymbol{\rho}}_{XYZ}^T \tag{17}$$

where

$$\tilde{\boldsymbol{\rho}} \equiv \int_0^\infty \mathrm{e}^{-st}\boldsymbol{\rho}\mathrm{d}t \tag{18}$$

The initial condition of the excited triplet state of D$-^3$A* can be described as

$$\boldsymbol{\rho}_{XYZ}^T(0) = \begin{matrix}\langle X| \\ \langle Y| \\ \langle Z|\end{matrix}\begin{pmatrix} p_X & 0 & 0 \\ 0 & p_Y & 0 \\ 0 & 0 & p_Z \end{pmatrix} \tag{19}$$

Unitary transforms of eqs 16 and 17 using $\mathbf{U}_T$ yield the following equations for the density matrices on the 123 basis systems.

$$s\tilde{\boldsymbol{\rho}}_{123}^T - \boldsymbol{\rho}_{123}^T(0) = -i[\hat{\mathrm{H}}_{123}^T, \tilde{\boldsymbol{\rho}}_{123}^T] - k_{ET}\tilde{\boldsymbol{\rho}}_{123}^T \tag{20}$$

$$s\tilde{\boldsymbol{\rho}}_{123}^{RP} - k_{ET}\tilde{\boldsymbol{\rho}}_{123}^T = -i[\hat{\mathrm{H}}_{123}^{RP}, \tilde{\boldsymbol{\rho}}_{123}^{RP}] \tag{21}$$

where

$$\boldsymbol{\rho}_{123}^T = \begin{matrix}\langle 1| \\ \langle 2| \\ \langle 3|\end{matrix}\begin{pmatrix} \rho_{11}^T & \rho_{12}^T & \rho_{13}^T \\ \rho_{21}^T & \rho_{22}^T & \rho_{23}^T \\ \rho_{31}^T & \rho_{32}^T & \rho_{33}^T \end{pmatrix} \tag{22}$$

$$\boldsymbol{\rho}_{123}^{RP} = \begin{matrix}\langle 1| \\ \langle 2| \\ \langle 3|\end{matrix}\begin{pmatrix} \rho_{11}^{RP} & \rho_{12}^{RP} & \rho_{13}^{RP} \\ \rho_{21}^{RP} & \rho_{22}^{RP} & \rho_{23}^{RP} \\ \rho_{31}^{RP} & \rho_{32}^{RP} & \rho_{33}^{RP} \end{pmatrix} \tag{23}$$

and

$$\boldsymbol{\rho}_{123}^T(0) = \mathbf{U}_T^{-1}\boldsymbol{\rho}_{XYZ}^T(0)\mathbf{U}_T \tag{24}$$

Equation 24 indicates that the initial condition of the density matrix of the excited triplet state in the presence of the magnetic field is simply determined by the unitary transform of the density matrix of eq 19 using $\mathbf{U}_T$.

By the inverse Laplace transform of eq 20, the following time dependence of the diagonal ($\boldsymbol{\rho}_{ii}^T$) and the off-diagonal ($\boldsymbol{\rho}_{ij}^T$) terms are obtained for ρ_{123}^T

$$\boldsymbol{\rho}_{ii}^T = \boldsymbol{\rho}_{123}^T(0)_{ii}\exp(-k_{ET}t) \tag{25}$$

$$\boldsymbol{\rho}_{ij}^T = \boldsymbol{\rho}_{123}^T(0)_{ij}\exp(-k_{ET}t)\exp\{-i(\omega_i - \omega_j)t\} \tag{26}$$

for $i = 1,2,3$ and $j = 1,2,3$ with $i \neq j$. In the following, two limiting cases, a and b, are considered to compute the ESP of the triplet CS state.

Case a: Fast Electron Transfer. When the k_{ET} value is much larger than the angular frequency of the Zeemann term of $g\beta B_0$, the coherence terms (off-diagonal terms) in $\boldsymbol{\rho}_{123}^T$ are not modulated by the angular frequency difference between the *i* and *j* levels because of $k_{ET} \gg |\omega_i - \omega_j|$ ($\approx g\beta B_0/\hbar$ in the case that the $|D_T|$ is smaller than the Zeeman energy) in eq 26. In this case, at the time ($s \ll k_{ET}$) when the ET reaction is completed, the initial condition $\boldsymbol{\rho}_{123}^{RP}(0)$ of the triplet CS state is simply treated as follows in eq 21 from eqs 18, 25, and 26

$$\boldsymbol{\rho}_{123}^{RP,fast}(0) \equiv k_{ET}\tilde{\boldsymbol{\rho}}_{123}^T = \boldsymbol{\rho}_{123}^T(0) \tag{27}$$

Thus, the density matrix for the CS state on the basis of the 1′, 2′, and 3′ levels is formulated as follows by using the relation of eq 4

$$\boldsymbol{\rho}_{1'2'3'}^{RP,fast} = \mathbf{U}_{CS}^{-1}\boldsymbol{\rho}_{123}^{RP,fast}(0)\mathbf{U}_{CS} \tag{28}$$

From eqs 13, 24, and 28, the density matrix for the triplet CS state is represented as follows

$$\boldsymbol{\rho}_{1'2'3'}^{RP,fast} = \mathbf{U}_{RP}^{-1}\mathbf{U}_{M'}^{-1}\boldsymbol{\rho}_{XYZ}^T(0)\mathbf{U}_{M'}\mathbf{U}_{RP} \tag{29}$$

When the ET rate is much larger than the angular frequency of the Zeemann interaction, one can see that the ESPT takes place through the zero-field basis systems as represented by $\mathbf{U}_{M'}{}^{-1}\boldsymbol{\rho}_{XYZ}^T(0)\mathbf{U}_{M'}$ (Figure 2a → Figure 2c) in eq 29 and that the populations in the sublevels of 1′, 2′, and 3′ in the CS state are distributed according to the coefficients of the wave functions described in eq 6.

Case b: Slow Electron Transfer. When the k_{ET} value is much smaller than the angular frequency of $g\beta B_0$, the coherence terms (off-diagonal terms) in ρ_{123}^T effectively undergo the quantum oscillations because of $k_{ET} \ll |\omega_i - \omega_j|$ ($\approx g\beta B_0/\hbar$) in eq 26. In this case, one can see from eqs 18 and 26 that the coherence terms in the transferred density matrix of $k_{ET}\tilde{\boldsymbol{\rho}}_{123}^T$ in eq 21 are averaged to be zero at the time ($s \ll k_{ET}$) when the ET is completed as follows

$$k_{ET}\tilde{\boldsymbol{\rho}}_{ij}^{T,slow} = 0 \tag{30}$$

with $i \neq j$. In the diagonal terms, one can obtain the following populations from eqs 18, 24, and 25,

$$k_{ET}\tilde{\boldsymbol{\rho}}_{ii}^{T,slow} = \boldsymbol{\rho}_{123}^{T}(0)_{ii} = |c_{iX}|^2 p_X + |c_{iY}|^2 p_Y + |c_{iZ}|^2 p_Z \equiv \rho_{ii} \tag{31}$$

Thus, the transferred density matrix in eq 21 can be described at the time when the ET reaction is completed as follows

$$\boldsymbol{\rho}_{123}^{RP,slow}(0) \equiv k_{ET}\tilde{\boldsymbol{\rho}}_{123}^{T,slow} = \begin{pmatrix} \rho_{11} & 0 & 0 \\ 0 & \rho_{22} & 0 \\ 0 & 0 & \rho_{33} \end{pmatrix} \tag{32}$$

From eqs 4 and 21, the density matrix for the triplet CS state on the basis of the 1′, 2′, and 3′ levels is then formulated as follows

$$\boldsymbol{\rho}_{1'2'3'}^{RP,slow} = \mathbf{U}_{CS}^{-1}\boldsymbol{\rho}_{123}^{RP,slow}(0)\mathbf{U}_{CS} = \mathbf{U}_{RP}^{-1}\mathbf{U}_{M'}^{-1}\mathbf{U}_{T}\begin{pmatrix} \rho_{11} & 0 & 0 \\ 0 & \rho_{22} & 0 \\ 0 & 0 & \rho_{33} \end{pmatrix}\mathbf{U}_{T}^{-1}\mathbf{U}_{M'}\mathbf{U}_{RP} \tag{33}$$

Since the coherence terms ρ_{ij} of the precursor triplet state in the 123 basis system are not transferred to the CS state when $k_{ET} \ll g\beta B_0/\hbar$, the density matrix of eq 33 in the CS state is different from the density matrix of the fast ET case of eq 29, resulting in the different ESP on the triplet CS state from the ESP by case a. When the high-field approximation that the spin-dipolar interactions are quite small with respect to the Zeeman interaction is applied both for the excited triplet state and for the triplet CS state, $\mathbf{U}_T \approx \mathbf{U}_{M'}\mathbf{U}_{RP}$ is obtained by eq 5 and eq 9 with using eq 8 and eq 12, respectively. With this relation and with eq 33, the populations in the CS states are approximated, as follows.

$$\rho_{1'1'}^{RP,slow} \approx \rho_{11},\ \rho_{2'2'}^{RP,slow} \approx \rho_{22},\ \rho_{3'3'}^{RP,slow} \approx \rho_{33} \tag{34}$$

When $k_{ET} \ll g\beta B_0/\hbar$, the triplet sublevel populations (in 1, 2, and 3 states in Figure 2b) are reflected on the sublevel populations (in 1′, 2′, and 3′ states in Figure 2d) in the CS state through the ET process. Once the triplet spin polarization characterized by $\rho_{11} - \rho_{33}$ is generated after the effective averaging of the off-diagonal terms due to the slow reaction in the laboratory frame, the absorptive or emissive spin polarization determined by $\rho_{11} - \rho_{33}$ is converted to the CS state through the ESPT, resulting in the net spin polarization by the TM that is represented as $\rho_{1'1'}{}^{RP} - \rho_{3'3'}{}^{RP} \approx \rho_{11} - \rho_{33}$ by eq 34. On the other hand, when the ET process is too fast to average the quantum coherences, the off-diagonal terms in the presence of the field are allowed to participate in the populations in $\rho_{1'1'}{}^{RP}$ and in $\rho_{3'3'}{}^{RP}$ of the CS state according to eq 28, resulting in the absence of the net TM effect. This absence of the TM is equivalent to the fast ESPT through the molecular frame represented by $\mathbf{U}_{M'}{}^{-1}\boldsymbol{\rho}^{T}{}_{XYZ}(0)\mathbf{U}_{M'}$ in eq 29 before the external magnetic field is applied to the triplet molecule.

The effect of the off-diagonal terms on the triplet−triplet ESPT described above should clearly be distinguished from the coherence effect in the sequential electron transfer polarization (SETP) model in which the off-diagonal terms in the singlet−triplet ($S-T_0$) system developed at the primary CS state is transferred as the radical pair mechanism (RPM) CIDEP to the population terms in the secondary SCRP levels by the ET reactions.[3,24,44–46,54] A significant difference between the present triplet ESPT and the SETP is that the frequencies ($\sim 10^{10}$ Hz in the X band spectrometer) of the quantum beats in the excited triplet state are extremely higher than the oscillation frequencies (typically $\sim 10^7$ Hz) in the $S-T_0$ system of the primary CS state since the energy splittings are mostly determined by the Zeeman interaction in the 1−2−3 system. Since the development of the coherence terms in the $S-T_0$ system is quite slow, the coherence terms are not averaged during the sequential ET taking place at the nanosecond time scale as an example, resulting in the RPM CIDEP effect in the RP state. On the other hand, by the ET processes with the nanosecond time scale, the coherence terms in the 1−2−3 system are completely averaged in the excited triplet state, resulting in the TM CIDEP determined only by the population terms in the precursor state. Indeed, in the present ESPT analysis, the precursor state does not undergo the coherent singlet−triplet interconversion between the excited singlet and the triplet state because of the extremely large exchange coupling in the excited states, denoting the validity of the 3 × 3 matrix representation described above.

B. Computation of the Electron Spin Polarization of the CS State. When the CS state in Figure 2d undergoes the singlet−triplet mixing between the states of $|S\rangle$ and $|2'\rangle$ to create the spin-correlated radical pair (SCRP) under the external magnetic field,[18] the four eigenstates are obtained as $|a\rangle = |1'\rangle$, $|b\rangle = \cos\mu\,|S\rangle + \sin\mu\,|2'\rangle$, $|c\rangle = -\sin\mu\,|S\rangle + \cos\mu\,|2'\rangle$, and $|d\rangle = |3'\rangle$ under the high B_0 limit. We assume that the response time of the EPR spectrometer is slower than the phase memory time or than the quantum oscillations in the $|a\rangle-|b\rangle-|c\rangle-|d\rangle$ system in which the density matrix of $\boldsymbol{\rho}_{abcd}$ is expressed by a 4 × 4 matrix on the basis of $|a\rangle|b\rangle|c\rangle|d\rangle$. The initial density matrix of $\boldsymbol{\rho}_{abcd}^{0}$ generated by the ESPT is represented using the above SCRP wave functions as follows

$$\boldsymbol{\rho}_{abcd}^{0} = \begin{matrix} \langle a| \\ \langle b| \\ \langle c| \\ \langle d| \end{matrix} \begin{pmatrix} \rho_{1'1'}^{RP} & \rho_{1'2'}^{RP}\sin\mu & \rho_{1'2'}^{RP}\cos\mu & \rho_{1'3'}^{RP} \\ \rho_{2'1'}^{RP}\sin\mu & \rho_{2'2'}^{RP}\sin^2\mu & \rho_{2'2'}^{RP}\cos\mu\sin\mu & \rho_{2'3'}^{RP}\sin\mu \\ \rho_{2'1'}^{RP}\cos\mu & \rho_{2'2'}^{RP}\cos\mu\sin\mu & \rho_{2'2'}^{RP}\cos^2\mu & \rho_{2'3'}^{RP}\cos\mu \\ \rho_{3'1'}^{RP} & \rho_{3'2'}^{RP}\sin\mu & \rho_{1'2'}^{RP}\cos\mu & \rho_{3'3'}^{RP} \end{pmatrix} \begin{matrix} \\ |a\rangle \\ |b\rangle \\ |c\rangle \\ |d\rangle \end{matrix} \tag{35}$$

where $\rho_{i'i'}^{RP}$ denotes the diagonal element (or population in Figure 2d) of $\boldsymbol{\rho}_{1'2'3'}^{RP,fast}$ or $\boldsymbol{\rho}_{1'2'3'}^{RP,slow}$ calculated by eq 29 or eq 33, respectively. Under the assumption of the slow response time, all of the off-diagonal elements that undergo the quantum oscillations can be treated to be zero in eq 35. Here, the angle μ is related as follows[24]

$$\cos\mu = \frac{2Q_-}{\sqrt{2\omega_2(\omega_2 - 2J - 2d)}}, \quad \sin\mu = \sqrt{\frac{\omega_2 - 2J - 2d}{2\omega_2}} \tag{36}$$

with $\omega_2 = [(2J + 2d)^2 + 4Q_-{}^2]^{1/2}$, where Q_-, $2J$ and $2d$ denote the Lamor frequency difference between radical 1 and radical

2, the spin−spin exchange interaction and the spin−spin dipolar interaction, respectively in the CS state. Q_- is represented using the g factors and hyperfine coupling constants (a) as,

$$Q_- = \frac{1}{2}\{(g_{1,\mathrm{eff}} - g_{2,\mathrm{eff}})\beta B_0 + \sum_m a_{1,m}M_{1,m} - \sum_n a_{2,n}M_{2,n}\} \tag{37}$$

In the CS state, the energy levels have been approximated under the high-field limit as follows[24]

$$\begin{aligned} \omega_a &= Q_+ + d - J \\ \omega_b &= -d + \frac{\omega_2}{2} \\ \omega_c &= -d - \frac{\omega_2}{2} \\ \omega_d &= -Q_+ + d - J \end{aligned} \tag{38}$$

where

$$Q_+ = \frac{1}{2}\{(g_{1,\mathrm{eff}} + g_{2,\mathrm{eff}})\beta B_0 + \sum_m a_{1,m}M_{1,m} + \sum_n a_{2,n}M_{2,n}\} \tag{39}$$

with

$$d = \frac{D'}{2}\left(\cos^2\theta_B - \frac{1}{3}\right) \tag{40}$$

As has been treated in Figure 3, when $g_X = g_Y$, the direction of the g_Z axis in the g tensor of one of the radicals in the CS state can be set by θ_g and ϕ_g as the polar angles with respect to the Z and the X axis, respectively. In this case, the effective g values in eq 37 and 39 can be obtained as follows[24]

$$g_{i,\mathrm{eff}} = \sqrt{g_{i,x}^2 e_X^2 + g_{i,y}^2 e_Y^2 + g_{i,z}^2 e_Z^2} \tag{41}$$

where

$$\begin{pmatrix} e_X \\ e_Y \\ e_Z \end{pmatrix} = \begin{pmatrix} \sin\phi_g & \cos\theta_g\cos\phi_g & \sin\theta_g\cos\phi_g \\ -\cos\phi_g & \cos\theta_g\sin\phi_g & \sin\theta_g\sin\phi_g \\ 0 & -\sin\theta_g & \cos\theta_g \end{pmatrix} \begin{pmatrix} \cos\phi_B\sin\theta_B \\ \sin\phi_B\sin\theta_B \\ \cos\theta_B \end{pmatrix} \tag{42}$$

By using the initial conditions of the diagonal elements in eq 35, time evolutions of the spin-state populations $\rho_{aa}(t)$, $\rho_{bb}(t)$, $\rho_{cc}(t)$, and $\rho_{dd}(t)$ have been computed with taking into account (1) the spin−lattice relaxations (for $|a\rangle$−$|b\rangle$, $|a\rangle$−$|c\rangle$, $|b\rangle$−$|d\rangle$, and $|c\rangle$−$|d\rangle$) to the thermal equilibrium populations, (2) the relaxations between $|b\rangle$ and $|c\rangle$ states corresponding to the dephasing between the $|S\rangle$ and the $|2'\rangle$ states induced by fluctuations of the exchange and the dipolar interactions,[23] and (3) the singlet charge-recombination from $|b\rangle$ and $|c\rangle$ states, as reported previously.[3,4] For the EPR transitions among the four levels, the transition intensities are represented under the weak microwave field strength as $I_{ab}(t) = [\rho_{bb}(t) - \rho_{aa}(t)]\sin^2\mu$, $I_{ac}(t) = [\rho_{cc}(t) - \rho_{aa}(t)]\cos^2\mu$, $I_{bd}(t) = [\rho_{dd}(t) - \rho_{bb}(t)]\sin^2\mu$, and $I_{cd}(t) = [\rho_{dd}(t) - \rho_{cc}(t)]\cos^2\mu$.[18] The time-dependent EPR spectra were computed by summing the above four transitions of a−b, a−c, b−c, and b−d obtained at all possible equally distributed molecular orientations of $\mathbf{\Omega}$ with respect to the direction of B_0.[4] The transverse magnetizations induced by the weak microwave field strength are represented as the powder pattern SP(t) of the EPR spectrum by the sum of the Lorentzian shape functions

$$\mathrm{SP}(t) = \int_0^{2\pi}\int_0^{\pi}\sum_{k,l}\mathrm{Im}\frac{I_{kl}(t)}{\omega_k - \omega_l + \omega_0 - \frac{i}{T_2}}|\sin\theta_B|\mathrm{d}\varphi_B\mathrm{d}\theta_B \tag{43}$$

where ω_k denotes the energy levels in the unit of angular frequency of the a, b, c, and d levels in the CS state in eq 38. ω_0 is the angular frequency of the microwave.

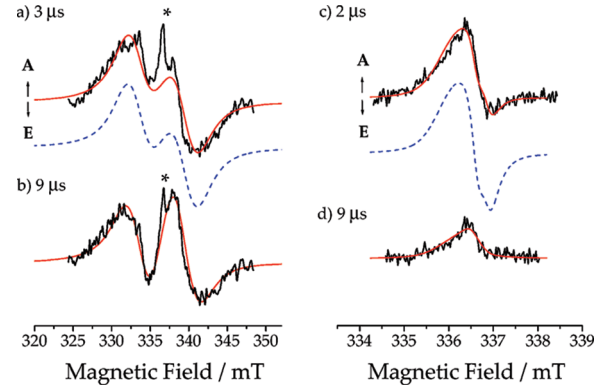

Figure 4. TREPR spectra of the photoinduced CS states of $ZnP^{+\bullet}$−$C_{60}^{-\bullet}$ at several delay times after the 532 nm laser irradiations at $T = 91$ K in benzonitrile. (a) and (b) The spectra exhibit the broad components and the narrow ones as marked by asterisks at the center field area. (c) and (d) The narrow components are recorded from 334.5 to 338 mT after subtracting the broad components by baseline corrections. (See text.) Red solid lines are obtained by the computer simulations of the ESPT with the slow ET model of eq 33 in which the triplet mechanism effect is included for the folded (left) and the extended (right) molecular geometries of the $ZnP^{+\bullet}$−$C_{60}^{-\bullet}$. Blue dashed lines were calculated with the fast ET model of eq 29.

Results and Discussion

A. TREPR Spectra. Figure 4 shows the TREPR spectra of the photoinduced CS states of $ZnP^{+\bullet}$−$C_{60}^{-\bullet}$ obtained by the 532 nm laser irradiations of the dyad molecule in Figure 1 at 91 K. As has been reported in the previous study,[4] in Figure 4a and 4b, both the broad spectra and the sharp ones shown by asterisks in Figure 4a and 4b are observed and are assigned to the CS states of the folded and the extended conformations, respectively. This is because the entire width of the spectrum is affected by the magnitude of the spin-dipolar interaction between the unpaired electrons of the RP in the solid state. In the broad component, the spectrum pattern changes from A/E-type polarization (Figure 4a) to the A/E/A/E polarization (Figure 4b), where A and E denote the microwave absorption and the emission, respectively. This spectrum change by the delay time was explained by a combination of the spin relaxation between the $|b\rangle$−$|c\rangle$ states and the singlet charge-recombination in the SCRP.[4]

At 2 μs after the laser irradiation, a broad A/E polarized signal is observed and is assigned to a combination of the $^3C_{60}$* and the folded CS state as reported in our previous study. At the

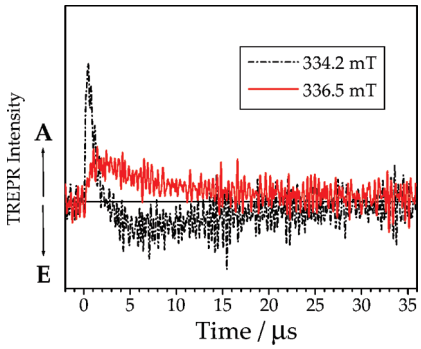

Figure 5. Time profiles of the TREPR signals at 334.2 and 336.5 mT obtained by the 532 nm laser irradiations at $T = 91$ K in benzonitrile.

field region from 334.5 to 339 mT, this broad spectrum can be approximated to be a linear line. (See Supporting Information for the TREPR signal at 2 μs.) Also, at 9 μs, the broad contribution can be approximated to be the linear-line spectrum around the center area from 334.5 to 338 mT in Figure 4b. Therefore, at 2 and 9 μs (Figure 4c and 4d), the sharp components can be obtained by subtracting the broad superimposed components using the linear-baseline functions obtained from the EPR intensities at 334.7 and 337.7 mT. One can see in Figure 4c that the net A polarization effect is imposed on the A/E-polarized component. The net A effect can be explained by the TM polarization generated by the CS reaction via the excited triplet state of ZnP$-^3$C$_{60}$*, i.e., ZnP$-^3$C$_{60}$* $\rightarrow$ ZnP$^{+\bullet}-$C$_{60}^{-\bullet}$ since a combination of (1) the negative D value and (2) the higher ISC rate to the X and Y levels than the rate for the Z level in the excited triplet state of fulleropyrollidine[28,55] can produce the absorptive ESP as the net TM effect.[34,56]

At 9 μs after the laser irradiation, the A/E component has mostly disappeared, while the net A contribution still exists. This is simply explained by the thermally equilibrium distribution in the SCRP levels due to the spin$-$lattice relaxations between the $a-b$, $a-c$, $b-d$, and $c-d$ levels, indicating that the singlet charge-recombination rate is smaller than the spin$-$lattice relaxation rate in the SCRP. Figure 5 shows the time profiles of the TREPR signals at 334.2 mT and at the center area of 336.5 mT in Figure 4c and 4d. The very quick rise of the 334.2 mT signal is attributed to the generation of the excited triplet state of ZnP$-^3$C$_{60}$* as has been reported in our previous study.[4] The time scale of the initial rise in the solid red line in Figure 5 is consistent with the decay time of the absorptive signal of ZnP$-^3$C$_{60}$*, strongly supporting that the CS state of the extended conformation is formed via ZnP$-^3$C$_{60}$* as described above. The absence of the oscillatory signals at the microsecond time window denotes that the quantum beats in the CS state systems disappeared because of the fast spin$-$spin relaxation or of the slow response time ($\sim$ 0.2 μs), indicating the validities in the treatments of eqs 35 and 43. The initial decay of the A polarization is attributable to the spin$-$lattice relaxation with a lifetime of $\sim$5 μs. After this decay, there still exists a weak absorptive polarization, indicating that the thermally equilibrium spin population is seen after ca. 10 μs. Decay of the absorptive signal is very slow (with a lifetime of >30 μs) and is due to the charge-recombination of the extended CS state. The rise of the emissive signal in the black dotted line in Figure 5 corresponds to the creation of the A/E/A/E polarization by a combination of the singlet CR and the spin relaxation processes, leading to estimation of the CR rate (k_{CR}) as shown in Table 1.

B. Simulations of the TREPR Spectra and Triplet Mechanism Effect by ESPT. In our previous study, the computer simulations of the TREPR spectra were performed for the folded geometry on the basis of the conventional ESPT theory that the triplet populations (ρ_{ii}^{RP}) in the CS state (Figure 2d) are equal to the probabilities finding the T_i ($i = X$, Y, and Z) characters of the precursor triplet state.[4] We have tried to simulate both of the TREPR spectra in Figure 4c and 4d by using the conventional ESPT model for the extended molecular conformation with a common set of parameters.[4,26] However, we were unable to reproduce the net A effect obtained at the initial stage (at 2 μs) at any set of the angle parameters of θ and ϕ. The net A effect is obtained when a smaller T_1 value ($\sim$2 μs) of the spin$-$lattice relaxation time is employed. However, the TREPR spectrum in Figure 4d is not reproduced with this parameter of $T_1 = 2$ μs. Instead of the conventional ESPT theory, the ESPT calculation of ρ_{ii}^{RP} has been performed by using the proposed theory described above for both of the folded and the extended conformations. The case (b) of eq 33 is applicable since the CS rate ($\sim 10^6$ s^{-1}) is much slower than the angular frequency of the Zeemann interaction in the present study. The time dependence of the EPR spectrum of eq 43 has been calculated by considering (1) the effect of T_{bc} as the spin-relaxation time between the $|b\rangle-|c\rangle$ states,[23] (2) the k_{CR} effect as the singlet charge-recombination rate in the SCRP, and (3) the spin$-$lattice relaxations characterized as T_1 between the $a-b$, $a-c$, $b-d$, and $c-d$ levels. The EPR parameters for the spectra simulations are reported in Table 1. By using the model of case (b), the time dependencies of the TREPR spectra are sufficiently reproduced both for the folded and for the extended geometries.

The spectrum calculation has also been undertaken (as shown under the spectra of Figure 4a and 4c) by considering the case (a) of eq 29 instead of eq 33. One can see that the net absorptive component is mostly absent in the dashed lines, while the net TM effects are well reproduced in the solid lines, demonstrating that the net effect in the SCRP is originating from the lack of the transfer of the coherence terms by the effective averaging by the quantum beats in the precursor triplet state as shown by eq 30.

C. Dipolar Parameters and Molecular Geometries of the CS States. On the extended conformation **2**, from the spin dipolar interaction of $D' = -0.25$ mT, the center-to-center distance between the unpaired spins is calculated by the point-dipole approximation to be $r_{SS} = 2.2$ nm. Figure 6 shows one of the extended structures of ZnP$-$C$_{60}$ geometrically optimized by the molecular mechanics calculation. From this molecular model, the center$-$center distance between the C$_{60}$ and the ZnP moieties is obtained to be 2.02 nm which is sufficiently in agreement with the point-dipole approximation of 2.2 nm. Also, with taking into account the principal axes (X, Y, and Z) of the dipolar interaction of the triplet fulleropyrollidine as reported in the previous studies,[55] the position of the ZnP moiety in the $X-Y-Z$ coordinate system is represented as $\theta = 53°$ and $\phi = -27°$ as shown in Figure 6. These angles are quite consistent with $\theta = 55°$ and $\phi = -30°$ obtained by the spectrum simulations of Figure 4c and 4d. Figure 7 shows calculated TREPR spectra obtained with different θ parameters of $\theta = 90°$, 40°, and 0° for the folded conformation **1** at 3 μs (Figure 7 left) and with θ values of $\theta = 90°$, 55°, and 30° for the extended conformation **2** at 2 μs (Figure 7 right) using eq 33. The other parameters for the calculations are fixed as listed in Table 1. It is clearly seen in Figure 7 that the ESP pattern is strongly affected by the angle of θ. We have obtained that the calculated ESP is also highly dependent on the angle ϕ. (See

TABLE 1: EPR Parameters for Spectrum Simulations (Red Lines in Figure [4]) of $ZnP^{+\bullet}-C_{60}^{-\bullet}$ for Folded and Extended Conformations[a]

	spin dipolar interaction			exchange interaction	spin−lattice relaxation times	relaxation time between $b-c$ levels		g-tensor components	
entry	D'/ mT	dipolar tensor orientations[b]	g tensor orientation[b]	$(2J)$/mT	$(T_1)/\mu$s	$(T_{bc})/\mu$s	$k_{CR}/10^5$ s^{-1}	$C_{60}^{-\bullet}$[c]	$ZnP^{+\bullet}$[d]
1 (folded)	−5.1	$\theta = 40°$ $\phi = 5°$	arbitrary	+2.0	10	3.0	10	$g_X = 2.00085$	2.00265
								$g_Y = 2.00038$	2.00265
2 (extended)	−0.25	$\theta = 55°$ $\phi = -30°$	$\theta_g = 45°$ $\phi_g = 0°$	+0.06	5.3	>20	0.31	$g_Z = 1.99925$	2.00220

[a] In $ZnP-{}^3C_{60}$*, the dipolar splitting parameters of $D_T = -9.17$ mT and $E_T = -1.32$ mT were used from reported values in fulleropyrollidine.[28] Sublevel-selecting ratios for the S_1-T_1 intersystem crossing were set to be $p_X = 0.67$, $p_Y = 0.33$, and $p_Z = 0.00$ for the X, Y, and Z levels, respectively.[28] [b] Polar angles of the Z' principal axes in the CS state with respect to the principal axes (X, Y, and Z) of the zero-field splitting interaction in $ZnP-{}^3C_{60}$*. [c] Reference 65. [d] Reference 33. Hyperfine couplings ($a_N = 0.196$ mT) from the four nitrogen atoms were considered in eqs 37 and 39.

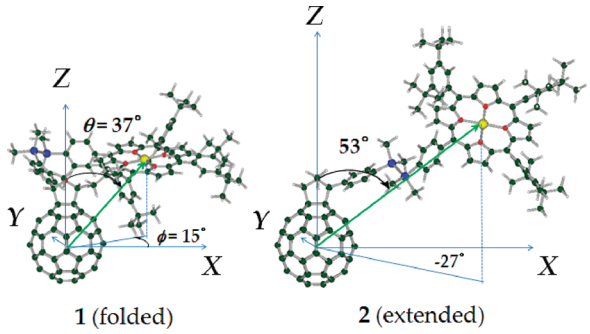

Figure 6. Molecular geometries of the (**1**) folded and (**2**) extended conformations obtained by the molecular mechanics calculations.

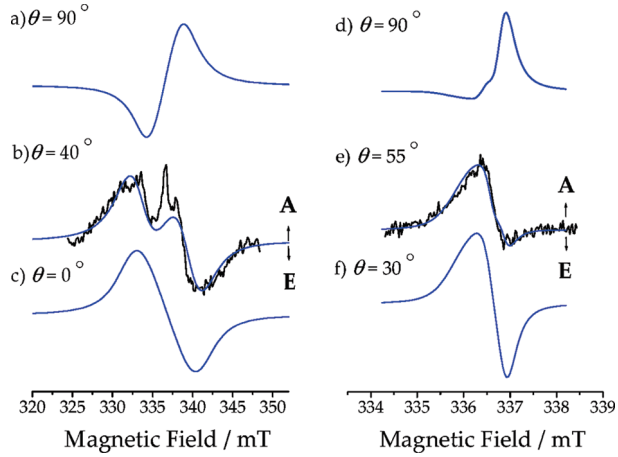

Figure 7. Dependence of the angle θ on the TREPR spectrum of the folded (a, b, and c) and the extended (d, e, and f) geometries. Experimental results in Figure 4a and 4c are shown by the black lines in b) and in e), respectively.

Supporting Information for the computed spectra.) Since the spin polarization pattern due to the ESPT is highly sensitive to the polar angles of θ and ϕ, the dipolar angles can be determined as listed in Table 1, characterizing the molecular geometries of the CS states with respect to the dipolar principal axes of the precursor triplet state. The molecular conformation obtained from the folded geometry **1** in Table 1 is also consistent with the molecular model (Figure 6 left) as reported in our previous study.[4]

D. Exchange Coupling and Its Connection to Mechanism of Electronic Coupling. Concerning the $2J$ of the CS states, the positive values are explained by the charge-transfer interaction as has been reported in numbers of CS state systems. According to the model, the singlet−triplet energy gap of $2J$ is generated by the spin-selective configuration interaction from the charge-recombined (CR) states such as the ground state of D−A.[29,57–61] Since the reorganization energy for the ET is small in the porphyrin−C_{60} systems,[62] CS energy level is located at the inverted region with respect to the ground state.[4] In this situation, when the CR to the excited triplet configuration is negligible, the $2J$ is approximated as follows[4,29,59]

$$2J = \frac{|V_{CR}|^2}{\Delta E_{CR}} \tag{44}$$

where $|V_{CR}|$ denotes the electronic coupling. ΔE_{CR} is the vertical energy gap for the charge-recombination and is represented as $\Delta E_{CR} = -\Delta G_{CR} - \lambda$ where ΔG_{CR} and λ denote the free energy change for the CR and the total reorganization energy, respectively. From Table 1, the $2J$ of 0.06 mT obtained for the extended conformation is about 30 times smaller than $2J = 2.0$ mT for the folded conformation. This is explained by the difference in $|V_{CR}|$ since the center-to-center distance between the unpaired electrons is different between the folded ($r_{SS} = 0.8$ nm)[4] and the extended conformation ($r_{SS} = 2.2$ nm). According to the ET theory, the CR reaction rate is formulated as follows[63]

$$k_{CR} = \frac{2\pi}{\hbar}|V_{CR}|^2 \frac{1}{\sqrt{4\pi\lambda k_B T}} \exp\left(-\frac{\Delta E_{CR}^2}{4\lambda k_B T}\right) \tag{45}$$

It is noteworthy that k_{CR} of the singlet CR rate in Table 1 is also about 30 times smaller in the extended conformation than in the folded conformation. This result is in good agreement with the difference in the $2J$ values, reflecting the difference in $|V_{CR}|$ in eq 45 by the molecular geometry. The above arguments clearly show that the parameters of the exchange coupling and the chemical kinetics are reasonable, demonstrating the validity of the computational analysis of the ESPT model of eq 33 which is proposed in the present study.

In our previous study, $|V_{CR}| = 4$ cm^{-1} has been estimated from $2J = 2.0$ mT using eq 44 for the folded conformation.[4] Assuming that the ΔE_{CR} (~1 eV) is constant for both of the molecular conformations,[4] $|V_{CR}| = 0.7$ cm^{-1} is obtained from the $2J$ of 0.06 mT for the extended conformation. (See Supporting Information for details of the estimation of ΔE_{CR}.) This electronic coupling $|V_{CR}| = 0.7$ cm^{-1} is explained in terms

of the bridge-mediated, superexchange mechanism through the diphenyldisilane linker[52] since the direct through-space overlap is negligibly small for the extended conformation with r_{SS} = 2.2 nm, while the though-space interaction is operative for the folded geometry (r_{SS} = 0.8 nm) as reported in our previous study.[4] Although the r_{SS} values are quite different between the folded and extended geometries, the $|V_{CR}|$ value of 4 cm^{-1} in the folded conformation is similar in order of magnitude with $|V_{CR}| = 0.7$ cm^{-1} of the extended geometry, indicating that the electronic interaction for the folded geometry is very weak. This relatively small $|V_{CR}|$ value has been explained by the orthogonal relationship between the active SOMOs of the π-orbitals in $ZnP^{+\bullet}$ and in $C_{60}^{-\bullet}$.[4]

In the previous TREPR study on a primary CS state ($ZnP-H_2P^{+\bullet}-C_{60}^{-\bullet}$) of a triad of the ZnP-free base porphyrin$-C_{60}$ ($ZnP-H_2P-C_{60}$) system bridged by diphenylamide ($-Ph-CONH-Ph-$) spacers, $|V_{CR}| = 1.6$ cm^{-1} has been determined from the exchange coupling in the radical pair of $-H_2P^{+\bullet}-Ph-CONH-Ph-C_{60}^{-\bullet}$.[3] $|V_{CR}| = 0.7$ cm^{-1} in the present system is smaller than the electronic coupling of 1.6 cm^{-1} mediated by the $-Ph-CONH-Ph-$ spacer, although the number of bonds to mediate the superexchange coupling by the diphenyldisilane linker is the same as the bond number for the diphenylamide linker. These results are quite consistent with the recent observations that the photoinduced CS rate ($k_q = 2.8 \times 10^9$ s^{-1}) of the dyad of $^1ZnP^*-C_{60}$ linked by diphenyldisilane via the through-bond coupling is substantially smaller than the CS rate (9.5×10^9 s^{-1}) of the dyad of $^1ZnP^*-C_{60}$ linked by the diphenylamide spacer.[52] These differences in the electronic couplings caused by the bridges can be explained in terms of the superexchange mechanism.[3,52,64] Sasaki et al. calculated that the lowest unoccupied molecular orbital (LUMO) levels of 1,2-diphenyl-1,1,2,2-tetramethyldisilane and of *N*-phenylbenzamide are 2.88 and 2.25 eV, respectively, by using the density functional theory calculations.[52] The higher LUMO energy level in the diphenyldisilane moiety than in the *N*-phenylbenzamide denotes that the tunneling energy gap (ΔE_{tu}) between the virtual state of $D^{+\bullet}-bridge^{-\bullet}-A$ and the CS state is higher in the present system.[3,52] This is quite consistent with the weaker electronic interaction in the present CS system than the electronic coupling in the reported CS state of $-H_2P^{+\bullet}-Ph-CONH-Ph-C_{60}^{-\bullet}$. The above arguments strongly support that the exchange couplings obtained for the CS states are quite reasonable, demonstrating that the proposed ESPT theory in this study is powerful to clarify both the molecular geometry and the electronic coupling of the photoinduced CS state produced via the spin-polarized excited triplet configuration in the donor$-$bridge$-$acceptor systems.

Summary

We have proposed the theoretical model of the ESPT by the photoinduced CS reaction via the excited triplet state. It has generally been shown here that the triplet ESP of the CS state is represented by the unitary transformation of the density matrix of the excited triplet state in the presence of the external magnetic field. When the triplet precursor CS reaction is faster than the time scale of the quantum oscillation occurring largely by the Zeeman frequency, the coherence terms in the precursor triplet state are conserved to be transferred to the CS state, resulting in the symmetric polarized TREPR spectra as shown by dashed lines in Figure 4. Contrarily, when the CS reaction is much slower than the quantum oscillation under the external magnetic field, the coherence terms in the density matrix of the triplet state are averaged by the effective oscillations to become zero during the time that the CS reaction takes place. This effect results in the generation of the triplet mechanism CIDEP in the CS state as seen in the solid lines in Figure 4a and 4c. The proposed theory is utilized to simulate the TREPR spectra of the photoinduced CS states of $ZnP-C_{60}$ dyads bridged by diphenyldisilane. The dipolar parameters (D, θ, and ϕ) and the exchange couplings ($2J$) are determined for both of the folded and the extended geometries and are revealed to be quite consistent with the molecular structures and the reported electronic interactions for the bridge-mediated superexchange mechanism. The present theoretical study strongly indicates that the proposed method to compute the ESPT is quite powerful to characterize the molecular geometry or orientation in the CS state system in the several D$-$A systems. This is because the TREPR spectra of the CS states are strongly dependent on (1) the anisotropic characters both in the intersystem crossing and in the zero-field splitting interaction of the triplet states and (2) the averaging of the quantum coherences in the excited triplet state resulting in the triplet mechanism CIDEP. Investigations of the distances, molecular orientations, and the exchange couplings of the CS states formed by the triplet-precursor reaction systems are now in progress in several photoinduced CS states including protein systems.

Acknowledgment. Y.K. thanks Dr. Yuki Shibano, Professor Hayato Tsuji (The University of Tokyo), and Professor Kohei Tamao (RIKEN) for providing the dyad sample and for having fruitful discussions. Y.K. also thanks Mr. Hiroto Nagata (Shizuoka University) for useful discussions on the ESPT model. This work was supported by the Morino Foundation for Molecular Science and by a Grant-in-Aid for Scientific Research (No. 19614005) from Ministry of Education, Culture, Sports, Science and Technology, Japan. This research was partially carried out by using an instrument at the Center for Instrumental Analysis of Shizuoka University.

Supporting Information Available: TREPR spectra without baseline corrections around the center area in Figure 4a. Computations of the dependence of the angle ϕ on the TREPR spectrum of the CS state and the estimations of the vertical energy gap for the CR processes. This material is available free of charge via the Internet at http://pubs.acs.org.

References and Notes

(1) Wasielewski, M. R. *J. Org. Chem.* **2006**, *71*, 5051–5066.
(2) Fukuzumi, S. *Phys. Chem. Chem. Phys.* **2008**, *10*, 2283–2297.
(3) Kobori, Y.; Yamauchi, S.; Akiyama, K.; Tero-Kubota, S.; Imahori, H.; Fukuzumi, S.; Norris, J. R. *Proc. Natl. Acad. Sci. U.S.A.* **2005**, *102*, 10017–10022.
(4) Kobori, Y.; Shibano, Y.; Endo, T.; Tsuji, H.; Murai, H.; Tamao, K. *J. Am. Chem. Soc.* **2009**, *131*, 1624–1625.
(5) Yang, S. I.; Seth, J.; Balasubramanian, T.; Kim, D.; Lindsey, J. S.; Holten, D.; Bocian, D. F. *J. Am. Chem. Soc.* **1999**, *121*, 4008–4018.
(6) Davis, W. B.; Svec, W. A.; Ratner, M. A.; Wasielewski, M. R. *Nature* **1998**, *396*, 60–63.
(7) Shaakov, S.; Galili, T.; Stavitski, E.; Levanon, H.; Lukas, A.; Wasielewski, M. R. *J. Am. Chem. Soc.* **2003**, *125*, 6563–6572.
(8) Wasielewski, M. R. *Chem. Rev.* **1992**, *92*, 435–461.
(9) Gust, D.; Moore, T. A.; Moore, A. L. *Acc. Chem. Res.* **2001**, *34*, 40–48.
(10) Imahori, H.; Tamaki, K.; Guldi, D. M.; Luo, C. P.; Fujitsuka, M.; Ito, O.; Sakata, Y.; Fukuzumi, S. *J. Am. Chem. Soc.* **2001**, *123*, 2607–2617.
(11) Fukuzumi, S.; Kotani, H.; Ohkubo, K.; Ogo, S.; Tkachenko, N. V.; Lemmetyinen, H. *J. Am. Chem. Soc.* **2004**, *126*, 1600–1601.
(12) Di Valentin, M.; Bisol, A.; Agostini, G.; Fuhs, M.; Liddell, P. A.; Moore, A. L.; Moore, T. A.; Gust, D.; Carbonera, D. *J. Am. Chem. Soc.* **2004**, *126*, 17074–17086.
(13) Feher, G.; Allen, J. P.; Okamura, M. Y.; Rees, D. C. *Nature* **1989**, *339*, 111–116.

(14) Wong, S. K.; Hutchins, Da; Wan, J. K. S. *J. Chem. Phys.* **1973**, *58*, 985–989.
(15) Pedersen, J. B.; Freed, J. H. *J. Chem. Phys.* **1973**, *58*, 2746–2761.
(16) Hore, P. J.; McLauchlan, K. A. *J. Magn. Reson.* **1979**, *36*, 129–134.
(17) Buckley, C. D.; Hunter, D. A.; Hore, P. J.; McLauchlan, K. A. *Chem. Phys. Lett.* **1987**, *135*, 307–312.
(18) Closs, G. L.; Forbes, M. D. E.; Norris, J. R. *J. Phys. Chem.* **1987**, *91*, 3592–3599.
(19) Murai, H.; Imamura, T.; Obi, K. *Chem. Phys. Lett.* **1982**, *87*, 295–298.
(20) Terazima, M.; Yamauchi, S.; Hirota, N. *Chem. Phys. Lett.* **1983**, *98*, 145–148.
(21) Di Valentin, M.; Agostini, G.; Salvadori, E.; Ceola, S.; Giacometti, G. M.; Hiller, R. G.; Carbonera, D. *Biochim. Biophys. Acta* **2009**, *1787*, 168–175.
(22) Di Valentin, M.; Ceola, S.; Salvadori, E.; Agostini, G.; Carbonera, D. *Biochim. Biophys. Acta* **2008**, *1777*, 186−195.
(23) Fukuju, T.; Yashiro, H.; Maeda, K.; Murai, H.; Azumi, T. *J. Phys. Chem. A* **1997**, *101*, 7783–7786.
(24) Morris, A. L.; Snyder, S. W.; Zhang, Y. N.; Tang, J.; Thurnauer, M. C.; Dutton, P. L.; Robertson, D. E.; Gunner, M. R. *J. Phys. Chem.* **1995**, *99*, 3854–3866.
(25) Kothe, G.; Weber, S.; Ohmes, E.; Thurnauer, M. C.; Norris, J. R. *J. Phys. Chem.* **1994**, *98*, 2706–2712.
(26) Akiyama, K.; Tero-Kubota, S.; Ikoma, T.; Ikegami, Y. *J. Am. Chem. Soc.* **1994**, *116*, 5324–5327.
(27) Kothe, G.; Weber, S.; Bittl, R.; Ohmes, E.; Thurnauer, M. C.; Norris, J. R. *Chem. Phys. Lett.* **1991**, *186*, 474–480.
(28) Da Ros, T.; Prato, M.; Guldi, D. M.; Ruzzi, M.; Pasimeni, L. *Chem.—Eur. J.* **2001**, *7*, 816–827.
(29) Kobori, Y.; Sekiguchi, S.; Akiyama, K.; Tero-Kubota, S. *J. Phys. Chem. A* **1999**, *103*, 5416–5424.
(30) Scott, A. M.; Miura, T.; Ricks, A. B.; Dance, Z. E. X.; Giacobbe, E. M.; Colvin, M. T.; Wasielewski, M. R. *J. Am. Chem. Soc.* **2009**, *131*, 17655–17666.
(31) Carmieli, R.; Zeidan, T. A.; Kelley, R. F.; Mi, Q.; Lewis, F. D.; Wasielewski, M. R. *J. Phys. Chem. A* **2009**, *113*, 4691–4700.
(32) Dance, Z. E. X.; Ahrens, M. J.; Vega, A. M.; Ricks, A. B.; McCamant, D. W.; Ratner, M. A.; Wasielewski, M. R. *J. Am. Chem. Soc.* **2008**, *130*, 830–832.
(33) Fuhs, M.; Elger, G.; Mobius, K.; Osintsev, A.; Popov, A.; Kurreck, H. *Mol. Phys.* **2000**, *98*, 1025–1040.
(34) Atkins, P. W.; Evans, G. T. *Mol. Phys.* **1974**, *27*, 1633–1644.
(35) Norris, J. R.; Morris, A. L.; Thurnauer, M. C.; Tang, J. *J. Chem. Phys.* **1990**, *92*, 4239–4249.
(36) Muss, L. T.; Atkins, P. W.; McLauchlan, K. A.; Pedersen, J. B. *Chemically Induced Magnetic Polarization*; Reidel: Dordrecht, The Netherlands, 1977.
(37) Prisner, T. F.; Vanderest, A.; Bittl, R.; Lubitz, W.; Stehlik, D.; Mobius, K. *Chem. Phys.* **1995**, *194*, 361–370.
(38) vanderEst, A.; Prisner, T.; Bittl, R.; Fromme, P.; Lubitz, W.; Mobius, K.; Stehlik, D. *J. Phys. Chem. B* **1997**, *101*, 1437–1443.
(39) Stehlik, D.; Mobius, K. *Annu. Rev. Phys. Chem.* **1997**, *48*, 745–784.
(40) Levanon, H.; Mobius, K. *Annu. Rev. Biophys. Biomol. Struct.* **1997**, *26*, 495–540.
(41) Mobius, K. *Chem. Soc. Rev.* **2000**, *29*, 129–139.
(42) Hulsebosch, R. J.; Borovykh, I. V.; Paschenko, S. V.; Gast, P.; Hoff, A. J. *J. Phys. Chem. B* **2001**, *105*, 10146–10146.
(43) Poluektov, O. G.; Paschenko, S. V.; Utschig, L. M. *Phys. Chem. Chem. Phys.* **2009**, *11*, 6750–6756.
(44) Tang, J.; Utschig, L. M.; Poluektov, O.; Thurnauer, M. C. *J. Phys. Chem. B* **1999**, *103*, 5145–5150.
(45) Hulsebosch, R. J.; Borovykh, I. V.; Paschenko, S. V.; Gast, P.; Hoff, A. J. *J. Phys. Chem. B* **1999**, *103*, 6815–6823.
(46) Kandrashkin, Y. E.; Salikhov, K. M.; van der Est, A.; Stehlik, D. *Appl. Magn. Reson.* **1998**, *15*, 417–447.
(47) McGlynn, S. P.; Azumi, T.; Kinoshita, M. *Molecular Spectroscopy of the Triplet State*; Prentice Hall: NJ, 1969.
(48) Imamura, T.; Onitsuka, O.; Murai, H.; Obi, K. *J. Phys. Chem.* **1984**, *88*, 4028–4031.
(49) Imamura, T.; Onitsuka, O.; Obi, K. *J. Phys. Chem.* **1986**, *90*, 6741–6744.
(50) Di Valentin, M.; Biasibetti, F.; Ceola, S.; Carbonera, D. *J. Phys. Chem. B* **2009**, *113*, 13071–13078.
(51) Katagiri, S.; Kobori, Y. *Appl. Magn. Reson.* **2010**, *37*, 177–189.
(52) Sasaki, M.; Shibano, Y.; Tsuji, H.; Araki, Y.; Tamao, K.; Ito, O. *J. Phys. Chem. A* **2007**, *111*, 2973–2979.
(53) Carrington, A.; McLachlan, A. D. *Introduction to Magnetic Resonance*; Harper & Row: New York, 1967.
(54) Norris, J. R.; Morris, A. L.; Thurnauer, M. C.; Tang, J. *J. Chem. Phys.* **1990**, *92*, 4239–4249.
(55) Bortolus, M.; Prato, M.; van Tol, J.; Maniero, A. L. *Chem. Phys. Lett.* **2004**, *398*, 228–234.
(56) Muss, L. T.; Atkins, P. W.; McLauchlan, K. A.; Pedersen, J. B. *Chemically Induced Magnetic Polarization*; Reidel: Dordrecht, The Netherlands, 1977.
(57) Anderson, P. W. *Phys. Rev.* **1959**, *115*, 2–13.
(58) Lukas, A. S.; Bushard, P. J.; Weiss, E. A.; Wasielewski, M. R. *J. Am. Chem. Soc.* **2003**, *125*, 3921–3930.
(59) Weiss, E. A.; Ratner, M. A.; Wasielewski, M. R. *J. Phys. Chem. A* **2003**, *107*, 3639–3647.
(60) Weiss, E. A.; Ahrens, M. J.; Sinks, L. E.; Gusev, A. V.; Ratner, M. A.; Wasielewski, M. R. *J. Am. Chem. Soc.* **2004**, *126*, 5577–5584.
(61) Kobori, Y.; Akiyama, K.; Tero-Kubota, S. *J. Chem. Phys.* **2000**, *113*, 465–468.
(62) Imahori, H.; Tkachenko, N. V.; Vehmanen, V.; Tamaki, K.; Lemmetyinen, H.; Sakata, Y.; Fukuzumi, S. *J. Phys. Chem. A* **2001**, *105*, 1750–1756.
(63) Marcus, R. A.; Sutin, N. *Biochim. Biophys. Acta* **1985**, *811*, 265–322.
(64) McConnell, H. M. *J. Chem. Phys.* **1961**, *35*, 508–515.
(65) Zoleo, A.; Maniero, A. L.; Prato, M.; Severin, M. G.; Brunel, L. C.; Kordatos, K.; Brustolon, M. *J. Phys. Chem. A* **2000**, *104*, 9853–9863.

JP102330A